ACS APPLIED MATERIALS & INTERFACES

www.acsami.org

Research Article

Controlling the Morphology of Dynamic Thia-Michael Networks to Target Pressure-Sensitive and Hot Melt Adhesives

Katie M. Herbert, Neil D. Dolinski, Nicholas R. Boynton, Julia G. Murphy, Charlie A. Lindberg, S. J. Sibener, and Stuart J. Rowan*

Cite This: *ACS Appl. Mater. Interfaces* 2021, 13, 27471−27480

Read Online

ACCESS | Metrics & More | Article Recommendations | Supporting Information

ABSTRACT: A series of multistage (pressure-sensitive/hot melt) adhesives utilizing dynamic thia-Michael bonding motifs are reported. The benzalcyanoacetate Michael acceptors used in this work undergo bond exchange under ambient conditions without external catalysis, facilitating pressure-sensitive adhesion. A key feature of this system is the dynamic reaction-induced phase separation that lends reinforcement to the otherwise weakly bonded materials, enabling weak, repeatable pressure-sensitive adhesion under ambient conditions and strong adhesion when processed as a hot melt adhesive. By using different pairs of benzalcyanoacetate cross-linking units, the phase separation characteristics of the adhesives can be directly manipulated, allowing for a tailored adhesive response.

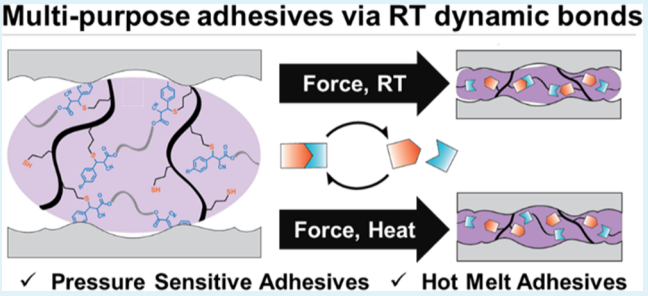

KEYWORDS: *dynamic covalent chemistry, pressure sensitive adhesive, hot melt adhesive, phase separation, rheology, thia-Michael bonds*

Downloaded via UNIV OF CHICAGO on January 21, 2022 at 21:03:13 (UTC).
See https://pubs.acs.org/sharingguidelines for options on how to legitimately share published articles.

INTRODUCTION

The scope of adhesive materials in daily life spans a vast range of targeted applications. From the biomedical to infrastructure sectors, modern adhesives are highly engineered to enable further functions that include conductivity,[1−4] biocompatibility,[5−7] degradability,[8−11] and smart adhesion.[12−14] In addition, these materials are traditionally subject to a range of mechanical property requirements depending on their desired purpose. For instance, pressure-sensitive adhesives (PSAs), such as those on the back of sticky notes or adhesive tapes,[15,16] require soft, viscoelastic solids for fast adhesion. Conversely, a hot melt adhesive (HMA) like a hot glue is designed to withstand large loads[17] and therefore necessitates the use of materials with high mechanical strength at typical operating temperatures. This expansive array of material requirements presents an intriguing opportunity to design new multipurpose adhesives that can be used in both pressure-sensitive and structural adhesive applications.

Recently, the integration of dynamic or reversible bonds into adhesive systems has shown considerable promise in developing a new generation of adhesive materials.[18−27] With applications ranging from underwater PSAs to rebondable structural adhesives, the dynamic bonds' ability to continuously break and reform in response to a stimulus without unwanted, irreversible side reactions[28−31] provides a means through which critical adhesion properties (i.e., surface wetting, adhesive bond formation) can be achieved (Figure 1a). Disulfide bonds have been particularly popular in accessing multifunctional HMAs on account of the bonds' ability to become dynamic to heat or UV light.[1,19,20,32−34] For example, both Michal et al.[23] and Cudjoe et al.[24] demonstrated the adhesive capabilities of dynamic covalent networks containing disulfide bonds. By disengaging the disulfide bonds using heat (>150 °C) or UV light, the modulus of the material lessened, allowing an adhesive bond to be formed between two glass or metallic substrates. Moreover, this adhesion was reversible, given the dynamic nature of the disulfide bond, and the bond could be reformed repeatedly even after failure. However, the stimuli used to reconfigure these systems (heat and UV light) limited the bonding substrate to either optically clear, UV inert materials or substrates that were capable of withstanding high temperatures (ca. 150 °C). These specifications effectively eliminate the disulfide dynamic networks as applicable adhesives for many common thermoplastics and room-temperature applications. To address these shortcomings, this work seeks to expand the utility of dynamic covalent adhesives through the use of dynamic bonds that undergo exchange at room temperature, with a particular focus on creating materials suitable for PSA applications.

Received: March 30, 2021
Accepted: May 24, 2021
Published: June 4, 2021

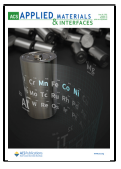

© 2021 American Chemical Society

https://doi.org/10.1021/acsami.1c05813
ACS Appl. Mater. Interfaces 2021, 13, 27471−27480

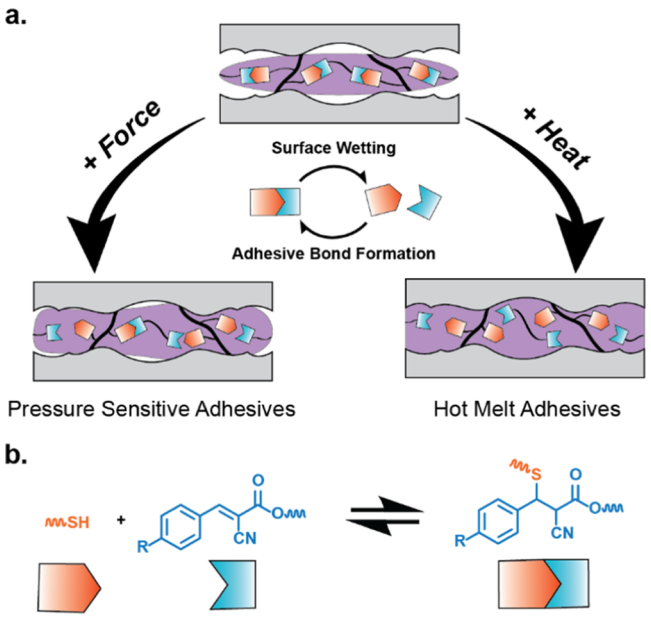

Figure 1. (a) Schematic illustration of dynamic covalent networks as adhesive materials. (b) Chemical scheme of generalized BCA-based tM reaction.

In order to effectively access room-temperature applications using dynamic network adhesives, the targeted equilibrium reaction should demonstrate reversible behavior in ambient conditions. Recent work by Bowman and co-workers has shown that (catalyzed) room-temperature thiol−thioester exchange can promote pressure-sensitive adhesion in thiol−ene adhesives, with further enhancement through pairing with hard filler particles.[35] The catalyst-free, room-temperature dynamic behavior of the thia-Michael (tM) bond (Figure 1b) based on benzalcyanoacetate (BCA) Michael acceptors makes it a promising candidate for dynamic covalent adhesives targeting applications at or near room temperature.[36−39] Recent studies have demonstrated the utility of the tM motif in polymeric networks toward creating responsive, reprocessible materials.[39−46] An interesting aspect of the BCA Michael acceptor structures is that the equilibrium constant with thiols can be directly tuned by controlling the electronic nature of the β-phenyl group. Importantly, neat dynamic networks based on the BCA structures demonstrated a dynamic reaction-induced phase separation (DRIPS) phenomenon, giving rise to materials with tunable amounts of a spontaneously formed, high thermal transition (>150 °C) hard phase.[38] Such materials were shown to have interesting stimuli responses (such as shape memory) and tunable mechanical properties that could be controlled based on thermal quenching from the melt, highlighting the ability to engineer material response by controlling the extent of phase separation. This phase separation management grants the ability to impart mechanical robustness into materials that otherwise would undergo significant flow in ambient conditions. With this in mind, the studies reported herein focus on leveraging the dynamic tM exchange at lower temperatures and the DRIPS morphology to simultaneously access low-strength, rebondable PSAs as well as high-strength HMAs.

RESULTS AND DISCUSSION

To take advantage of the desirable properties commonly exhibited by silicone-based PSAs (high-temperature stability, low glass transition temperatures, adhesion to low surface energy substrates[47]), a commercially available silicone polythiol, poly(mercaptopropyl methyl)siloxane (**PMMS**), was chosen as a bonding partner for dynamic BCA cross-linkers, **1** (Figure 2a). As the electronic nature of the β-phenyl substituent greatly impacts the dynamic equilibrium,[36,38] a series of cross-linkers were prepared with different −R groups, namely, the electron-donating −methoxy (**1M**), the electronically neutral −hydrogen (**1H**), and the electron-withdrawing −nitro (**1N**); see the Experimental Section for synthetic details. Using **PMMS** and **1X**, a series of dynamic polymer networks ($\mathbf{2N_{100}}$, $\mathbf{2N_{50}H_{50}}$, and $\mathbf{2N_{50}M_{50}}$, where the subscript denotes the mole percent (mol %) of the BCA crosslinkers (**1X**) relative to the total amount of thiol) were targeted (Figure 2b). In particular, these systems were chosen to probe the effects of varying equilibrium bonding position and DRIPS morphology on adhesive performance. Of particular interest is the comparison between $\mathbf{2N_{50}H_{50}}$ and $\mathbf{2N_{50}M_{50}}$ as it has been previously demonstrated that mixtures of **1N** and **1H** have an increased degree of phase separation in comparison to equivalent mixtures of **1N** and **1M**.[38] Additionally, the incorporation of more electron-donating cross-linkers (**1H** and **1M**) with strongly withdrawing cross-linkers (**1N**) effectively lowers the glass transition temperature (T_g) and plateau modulus as compared to a parent film composed completely of the stronger acceptor, yielding materials more suitable for pressure-sensitive adhesion (Figure S1).[38]

To obtain a baseline understanding of the equilibrium bonding behavior of the dynamic polymers, the equilibrium

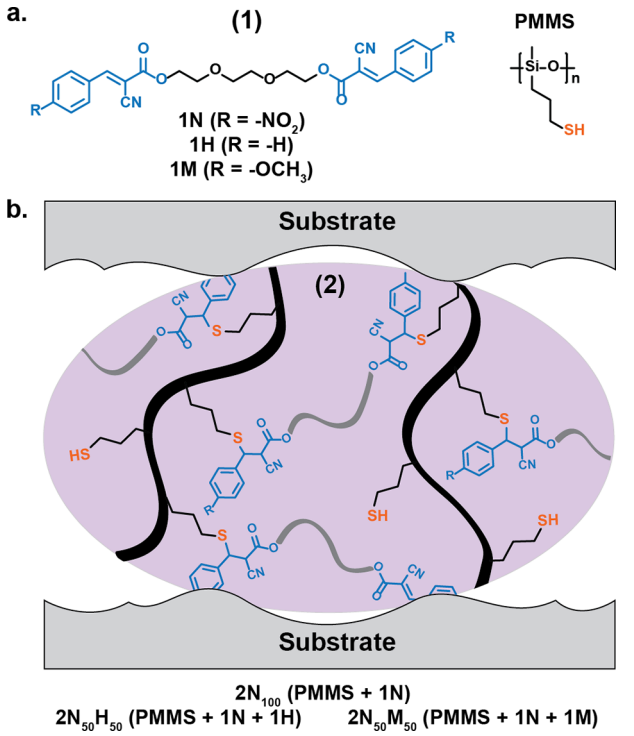

Figure 2. (a) Chemical structures of ditopic electrophiles (**1**) and **PMMS**. (b) Illustration demonstrating network (**2**) formation resulting from the combination of **PMMS** and **1**.

https://doi.org/10.1021/acsami.1c05813
ACS Appl. Mater. Interfaces 2021, 13, 27471−27480

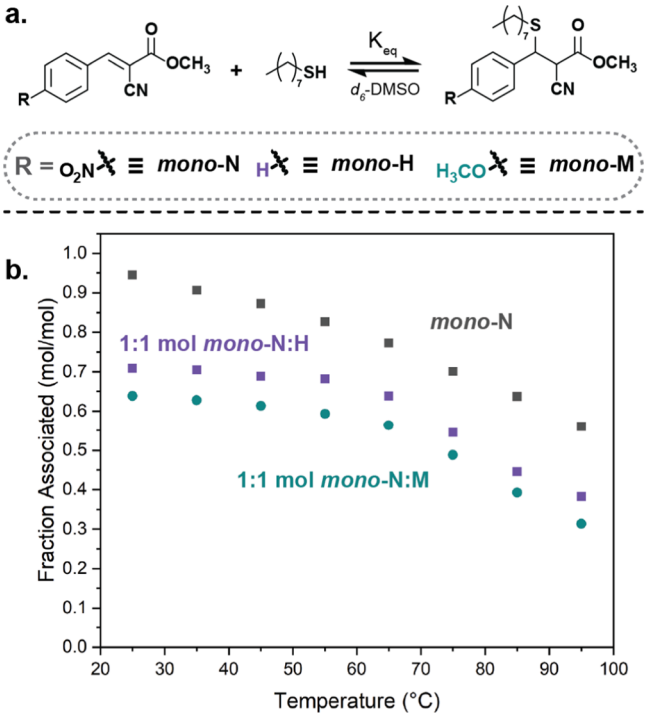

Figure 3. (a) Schematic of the small-molecule BCA Michael acceptors reaction with 1-octanethiol. (b) Equilibrium position of the bonding of 1 equiv (w.r.t. double bond) of 1-octanethiol with **mono-N** (black) or 1:1 mixtures of **mono-N** and either **mono-H** (violet) or **mono-M** (cyan) as a function of temperature in DMSO-d_6.

position of mixtures of small-molecule analogues (**mono-N**, **mono-H**, and **mono-M** for −nitro, −hydrogen, and −methoxy, respectively) with 1-octanethiol was carried out over a range of temperatures; see Figure 3a (Figures S2−S4). To simulate the materials, **mono-N** or equal mixtures of **mono-N** with either **mono-H** or **mono-M** were mixed with an equimolar concentration of thiol (200 mM concentrations of thiol, ∼10% of the concentration of the bulk films). As expected, the equilibrium position of the **mono-N** solution was higher than that of the either mixed system, with the **mono-N**/**mono-H** mixture showing a higher degree of equilibrium bonding than the **mono-N**/**mono-M** mixture for all temperatures (Figure 3b). It should be noted that despite this difference, the overall equilibrium position of both the mixed systems was quite similar (71 vs 64% at room temperature), largely a consequence of the competitive bonding between acceptors; see Figure S4 and Table S1. Interestingly, in both hybrid mixtures, the **mono-N** and **mono-H**/**M** acceptors displayed similar decreases in the equilibrium bonding position with increasing temperature as opposed to a preferential debonding of the "weaker" acceptor. This implies that changes in bonding upon heating should occur homogenously throughout the material, outside of phase-separated regions. The temperature-dependent equilibrium behavior also suggests that the overall network connectivity and the resulting adhesive properties will vary depending on the operating temperature.

The similarity in the measured equilibrium position of the model studies would suggest that the mechanical properties of $\mathbf{2N_{50}H_{50}}$ and $\mathbf{2N_{50}M_{50}}$ may be similar (assuming exchange kinetics occur over similar timescales). To investigate this, the viscoelastic properties of the dynamic networks were probed using small-amplitude oscillatory shear (SAOS) rheometry. Similar to previous findings,[38] temperature ramp experiments (Figure 4a) revealed two thermal transitions in all dynamic

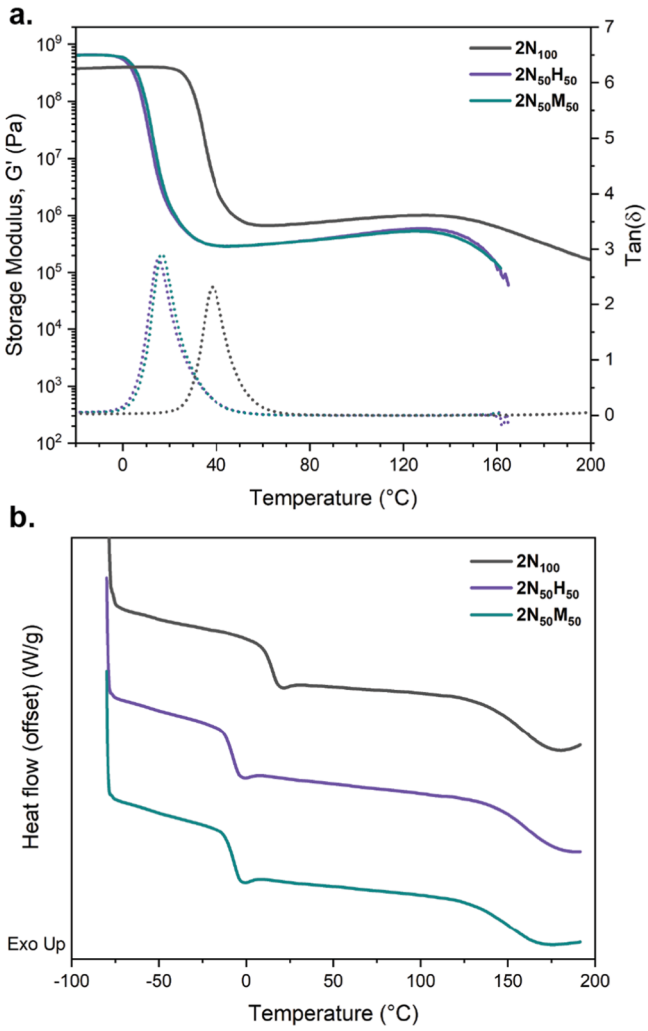

Figure 4. (a) Shear rheometry temperature ramps for $\mathbf{2N_{100}}$, $\mathbf{2N_{50}H_{50}}$, and $\mathbf{2N_{50}M_{50}}$ showing storage modulus (G', top) and tan δ (bottom) (ramp rate = 3 °C/min, frequency = 1 Hz). (b) DSC curves for tM films (ramp rate = 10 °C/min; heat/cool/heat cycle = 200 °C/−80 °C/200 °C; second heating shown).

networks. The first thermomechanical T_g (as defined by the tan δ peak) occurred below room temperature for both $\mathbf{2N_{50}H_{50}}$ and $\mathbf{2N_{50}M_{50}}$ at 15 and 16 °C, respectively, and above room temperature (∼40 °C) for $\mathbf{2N_{100}}$. Notably, the two hybrid samples exhibited a rubbery plateau modulus ranging from 2.8×10^5 to 5.8×10^5 Pa over a temperature range of more than 100 °C (ca. 40−140 °C), implying a large window of operation before the films begin to flow more readily. Importantly, above ∼140 °C, the two hybrid networks undergo a significant drop in modulus, thereby creating an opportunity for hot melt adhesion. $\mathbf{2N_{100}}$ also exhibits a drop in modulus at around this temperature, but the drop is less significant. Characteristic of bond dissociation in dynamic networks, the changes to moduli for all systems are accompanied by an increase in the loss modulus (Figure S5) before the samples begin to readily flow. Further thermal characterization of the films via differential scanning calorimetry (DSC) showed the presence of a second higher thermal transition (>150 °C)

https://doi.org/10.1021/acsami.1c05813
ACS Appl. Mater. Interfaces 2021, 13, 27471−27480

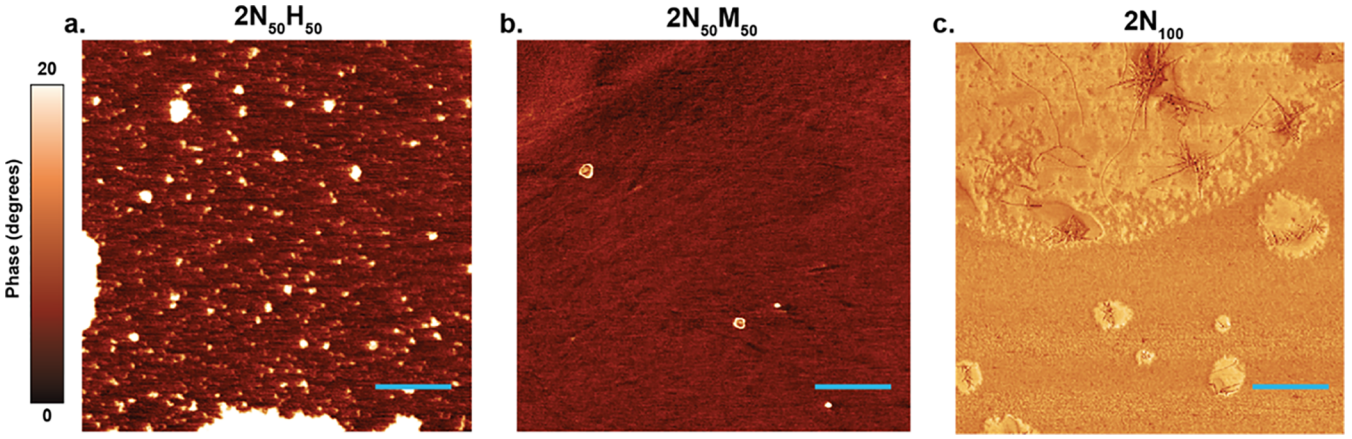

Figure 5. Atomic force micrographs showing the phase images of (a) $2N_{50}H_{50}$, (b) $2N_{50}M_{50}$, and (c) $2N_{100}$ samples (phase color scheme: dark = soft phase; light = hard phase; scale bar = 1 μm).

characteristic of a "hard phase" formed via DRIPS process (Figure 4b).[38]

To investigate the DRIPS morphology of the dynamic networks, atomic force microscopy (AFM) was carried out (at 0 °C for $2N_{50}H_{50}/2N_{50}H_{50}$ and 35 °C for $2N_{100}$), and the phase images are shown in Figure 5 (see Figures S6–S8 for height images). In line with prior work[38] on related systems, the $2N_{50}H_{50}$ (Figure 5a) sample showed significantly higher degrees of phase separation in comparison to $2N_{50}M_{50}$ (Figure 5b), though neither hybrid network displayed the large hard-phase domains found throughout $2N_{100}$ (Figure 5c). Interestingly, in the hybrid systems, the small hard-phase regions were largely disconnected, which potentially explains why the SAOS rheology was similar between $2N_{50}H_{50}$ and $2N_{50}M_{50}$, despite the difference in the hard-phase content. Taken together, the $2N_{50}H_{50}$ and $2N_{50}M_{50}$ networks have very similar continuous phases while differing starkly in the amount and distribution of hard phase throughout the material, representing an ideal system to assess the impact of DRIPS morphology on adhesive properties.

As an initial investigation into the adhesive properties of the DRIPS networks, SAOS frequency studies were used to further probe the PSA characteristics of the dynamic systems (Figure S9). Frequency sweeps from 0.01 to 100 rad/s were conducted at different temperatures centered around the target operating temperature of 25 °C. Using the time–temperature superposition principle (Figure S10), a master curve was generated at a reference temperature of 25 °C. Figure 6a shows the master curves for $2N_{50}H_{50}$ and $2N_{50}M_{50}$ as determined by multiple frequency sweeps shifted according to the WLF fit ($2N_{100}$ was determined to be too glassy at room temperature, Figure S11). Using these master curves, two principles were applied to define their ability to act as PSAs: the Dahlquist criterion and the viscoelastic window (VW). According to the Dahlquist criterion, for materials to be useful as PSAs, they should possess a storage modulus (G') less than 3×10^5 Pa (at 1.0 rad/s) at the operating temperature.[48] While it is clear that $2N_{50}M_{50}$ meets this criterion (dashed lines Figure 6a) at room temperature, $2N_{50}H_{50}$ has a modulus slightly higher than that would be ideal according to Dahlquist. While useful as a first approximation, the Dahlquist criterion serves only as a benchmark for PSAs. As such, Chang defined PSAs by identifying a VW within which PSA applications could be identified.[49] Using isothermal frequency studies, a VW is defined by the operating temperature storage and loss modulus (G'') at 0.01 and 100 rad/s. In a plot of storage vs loss modulus, the values can be used as coordinates to form four corners of a rectangle which constitutes the VW: (1) G' at 100 rad/s and G'' at 0.01 rad/s, (2) G' at 100 rad/s and G'' at 100 rad/s, (3) G' at 0.01 rad/s and G'' at 100 rad/s, and (4) G' at 0.01 rad/s and G'' at 0.01 rad/s. Their investigation determined that this window varies depending on the PSA application, and as a result, they were able to identify five viscoelastic regimes for PSAs based on the location of their VW in the G'/G'' plot: non-PSA (quadrant 1), high shear PSA (quadrant 2), removable PSA (quadrant 3), cold-temperature PSA (quadrant 4), and general PSA (central region). Using the frequency data acquired for the master curves, it was possible to establish VWs for $2N_{50}H_{50}$ and $2N_{50}M_{50}$. As shown in Figure 6b, much of the VW for $2N_{50}H_{50}$ and $2N_{50}M_{50}$ falls in quadrant 2, suggesting that the two materials would perform as high-shear PSAs. These types of PSAs are typically characterized by a high storage modulus which contributes to the higher shear strength relative to other PSAs. Generally, the differences in the VW for $2N_{50}H_{50}$ and $2N_{50}M_{50}$ highlight the ability to tune the adhesive response through manipulating the electronic nature of the dynamic bond, suggesting that future optimization of the dynamic network composition could target specific PSA applications. To assess the shear resistance of these adhesives, shear adhesion failure temperature (SAFT) tests with a 100 g hanging load were carried out. The SAFT measurements indicated failure temperatures of ~49 and ~54 °C for $2N_{50}H_{50}$ and $2N_{50}M_{50}$, respectively (Figure S12). The trend in the failure temperatures is consistent with the VW predictions, and the relatively low values are likely a consequence of accelerated dynamic exchange inducing creep in the adhesive.

Inspired by the potential adhesive characteristics of the tM films, the mechanical performance of these materials was assessed for both pressure-sensitive and hot melt adhesion. Three different testing methods were employed to evaluate the adhesive properties of the films: tack and 180-degree peel tests for probing their PSA abilities and normal force pull-off tests to determine their adhesive strength as HMAs. To assess the films as PSAs, the hybrid networks were prepared as tapes with Kapton backing on either side (see Experimental Section). To apply, the desired shape was cut from the tape, and the two Kapton sheets were pulled apart to expose the adhesive

https://doi.org/10.1021/acsami.1c05813
ACS Appl. Mater. Interfaces 2021, 13, 27471–27480

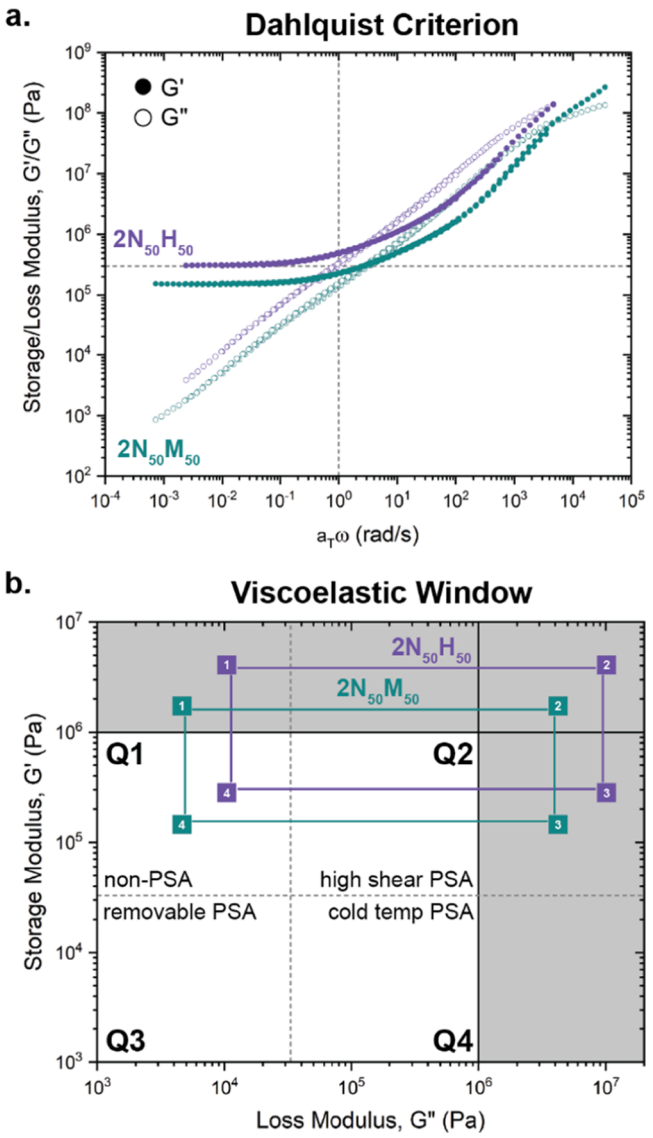

Figure 6. (a) Master curves from the WLF temperature shift factor (a_T) of SAOS rheology frequency studies for $2N_{50}H_{50}$ (violet) and $2N_{50}M_{50}$ (cyan) [amplitude (strain) = 1.0%; reference temperature = 25 °C]. Dashed lines highlight the Dahlquist criterion (3×10^5 Pa at 1 rad/s). (b) VWs for $2N_{50}H_{50}$ (violet) and $2N_{50}M_{50}$ (cyan) with corner numbers (1−4) corresponding to modulus values from master curves in plot a. Gray region highlights moduli outside of the typical VW plot.

material. This process served to protect the adhesive surface from contaminants and oxidation while also ensuring that the material was firmly attached to the Kapton substrate, facilitating an accurate measurement of PSA properties.

To begin assessing the PSA properties of the tM tapes, tack experiments were carried out. Samples were mounted onto the lower plate of a rheometer, and the top plate was pressed into the adhesive with a varied axial force (0.1, 1.0, and 10 N) for 10 s at room temperature. The force curve was then evaluated for both pull-off strength (peak force reached during the tack test) and adhesive/cohesive strength of tack (area under the force curve). As expected, higher applied force resulted in an increase in both the peak force and the adhesive tack strength (Figure 7a,b). Interestingly, both adhesives demonstrate similar peak forces across the range of applied forces. However, $2N_{50}M_{50}$ did demonstrate enhanced overall tack strength relative to $2N_{50}H_{50}$ with increasing applied force (Figure 7b).

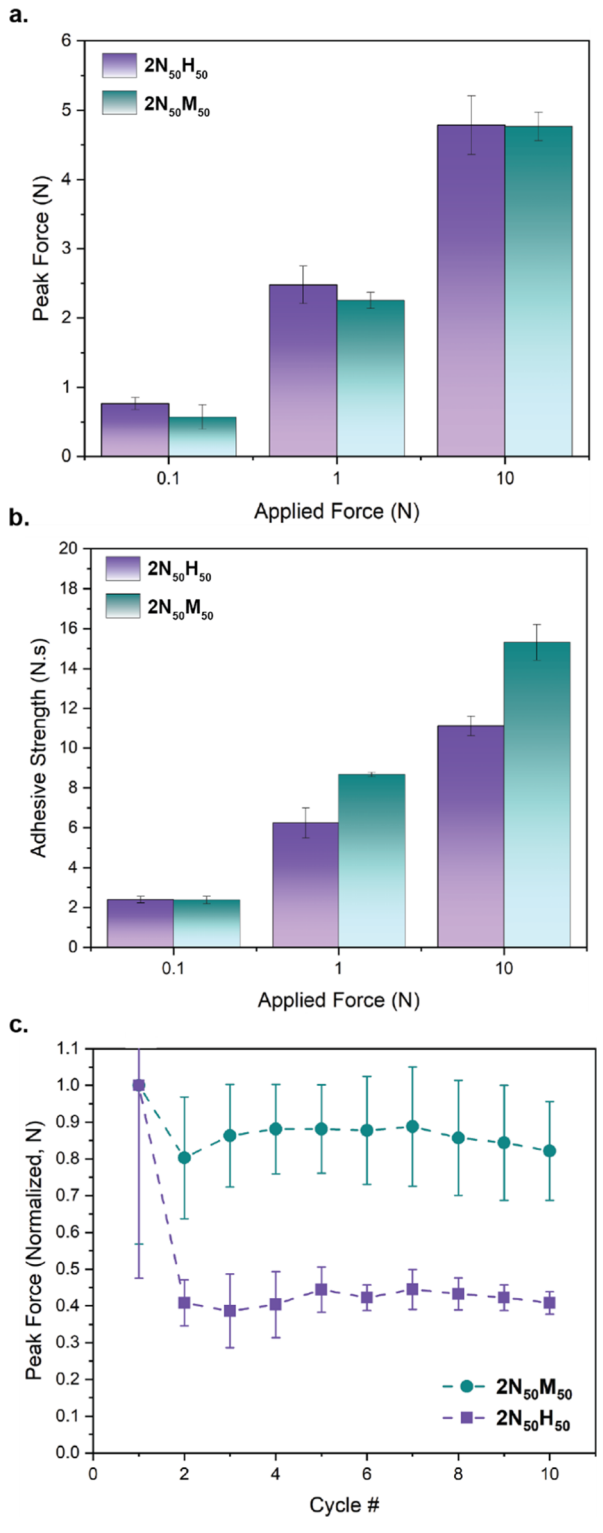

Figure 7. Graphical summary of the (a) peak force and (b) adhesive strength for tack test of $2N_{50}H_{50}$ (violet) and $2N_{50}M_{50}$ (cyan) with the variable applied force (8 mm parallel plate, 10 s application time, and 0.1 mm/s strain rate). (c) Graphical representation of the peak force for 10 consecutive repeat tack experiments on $2N_{50}H_{50}$ (squares) and $2N_{50}M_{50}$ (circles) (8 mm parallel plates, 0.1 mm/s strain rate, 60 s adhesion time, and 1.0 N applied force).

https://doi.org/10.1021/acsami.1c05813
ACS Appl. Mater. Interfaces 2021, 13, 27471−27480

This result is potentially a consequence of the resistance to flow of the larger amount of hard phase in $2N_{50}H_{50}$. As such, the tack strength of $2N_{50}H_{50}$ could be increased by extending contact times, presumably giving the hard-phase domains time to redistribute themselves (Figure S13). Interestingly, $2N_{100}$ (which was not suited for room-temperature PSA applications) did not yield measurable PSA performance even at elevated temperatures (up to 120 °C, Figure S14), presumably a result of a higher overall amount of large hard-phase domains relative to the mixed systems.

A critical parameter of PSAs is their ability to maintain their adhesive properties over several cycles. Generally speaking, a PSA functions under working conditions that are relatively short in adhesion time and small in applied force over the course of several bonding cycles. As such, the performance of the dynamic adhesives under cyclic loading conditions was assessed using a middling set of parameters (60 s adhesion time and 1 N applied force). Using the same tack test setup as previously described, samples of each material were tested for 10 consecutive tack cycles at room temperature (Figure 7c). Comparing the tack of the two materials, $2N_{50}H_{50}$ shows a stark drop in the peak force after the first bonding cycle, possibly arising from difficulties in rearranging the hard-phase domains after the initial loading conformation. Despite this drop in performance, it is important to note that both hybrid materials had overlapping values of peak tack force (~4.5 N) and tack strength (~15 N·s) for all cycles, excluding the first (Figure S15). These results highlight that both DRIPS adhesives displayed relatively consistent PSA characteristics over the course of repeated adhesions, demonstrating the rebondability of these materials.

Another useful metric for assessing the PSA performance is the peel strength. To investigate the peel performance of the DRIPS adhesives, the tapes were evaluated using a 180-degree peel test at room temperature. Prior to testing, the tapes were cut into rectangular strips and mounted onto a glass microscope slide, and a strip of aluminum foil was pressed onto the exposed adhesive surface. The foil strip was then peeled at a 180° angle from the top of the microscope slide, and the force was monitored (see the Experimental Section for complete details). As shown in Figure 8, $2N_{50}M_{50}$ consistently outperforms $2N_{50}H_{50}$ in peel strength. To put these peel results into an everyday context, identical experiments were carried out using double-sided stick tape (Scotch 3M), yielding average peel strength values of 0.24 ± 0.03 N/mm (Figure S16) comparable to the hybrid dynamic networks. Taken together with the tack test results, which demonstrate that the $2N_{50}M_{50}$ material is more able to flow upon exposure to brief, low-pressure forces (presumably a result of both the lower modulus of the continuous phase and the relatively small domains of the hard phase), $2N_{50}M_{50}$ is shown to exhibit a better overall performance as a general purpose, rebondable PSA. This agrees well with the rheological criteria as well: $2N_{50}M_{50}$ met the Dahlquist criterion and had a VW more suited to a PSA regime.

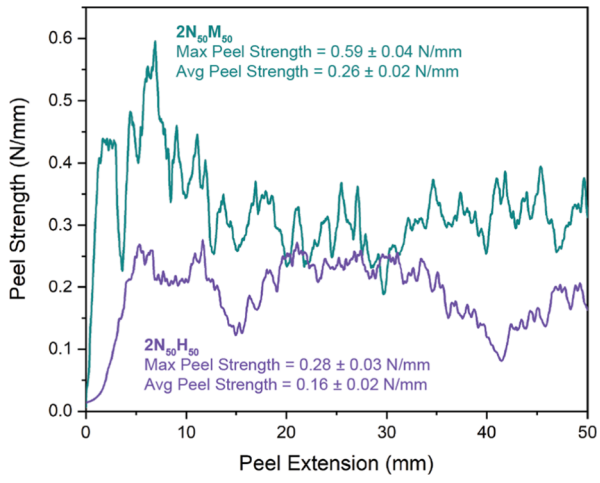

Figure 8. Representative peel test curves for $2N_{50}H_{50}$ (violet) and $2N_{50}M_{50}$ (cyan).

In addition to the utility of these materials as PSAs, the onset of macroscopic flow, the temperature-dependent dynamic exchange equilibrium, and the presence of reinforcing hard phase in the DRIPS adhesives imply that these materials would be able to operate as HMAs. By heating the DRIPS materials above ~150 °C, the molten adhesive can efficiently flow between substrates and, upon cooling, form bridging hard-phase domains that should lend significant strength to the bonded assembly. To evaluate their performance as HMAs, squares of the original pressed DRIPS films (not tape) were used to adhere two aluminum I-bars together at 180 °C. Once cooled, the two I-bars were loaded into a uniaxial tensile testing apparatus, and the adhesive strength of the film was determined (Figure 9a). The strongly bound $2N_{100}$ material, while unable to perform as a PSA due to the high glass transition temperature, performed impressively in a hot melt context, leading to high values of adhesive strength (0.80 ± 0.07 MPa). In agreement with the temperature ramp rheology studies, the $2N_{100}$ material did not undergo a significant amount of flow even when processed at 180 °C (Figure 9b). However, despite the glassy nature of $2N_{100}$, the samples failed cohesively, implying strong adhesion to the aluminum substrate.

Despite their ability to deform at room temperature, both $2N_{50}H_{50}$ and $2N_{50}M_{50}$ demonstrated impressive adhesive strengths when applied as HMAs, particularly $N_{50}H_{50}$, whose performance (0.81 ± 0.1 MPa) matched that of $2N_{100}$. In the case of both hybrid materials, the initial ~5 × 5 × 0.4 mm material underwent significant flow when processed at 180 °C, leaving much larger cohesive failure footprints (Figure 9c,d) than those left by $2N_{100}$, thereby acting as more efficient HMAs on a volumetric basis (force values in Figures 9a and S17b). The outstanding HMA performance of $2N_{50}H_{50}$ is largely a result of the relatively high amount of hard-phase domains throughout the sample, which efficiently dissolve/spread upon exposure to high temperatures and act to bridge substrates upon cooling. This result clearly demonstrates the potential impact of tuning the morphology of DRIPS-based adhesives, which enables the targeting of performance parameters ranging from low strength, rebondable PSAs to high-strength HMAs.

CONCLUSIONS

Hybrid tM networks composed of ditopic acceptor compounds (**1**) and an oligomeric thiol component (**PMMS**) demonstrated the ability to function as both PSAs and HMAs. Their viscoelastic behavior at room temperature met the Dahlquist criterion (modulus < 3×10^5 Pa at a testing frequency of 1.0 rad/s), indicating their potential for use as PSAs. Cyclic tack

https://doi.org/10.1021/acsami.1c05813
ACS Appl. Mater. Interfaces 2021, 13, 27471−27480

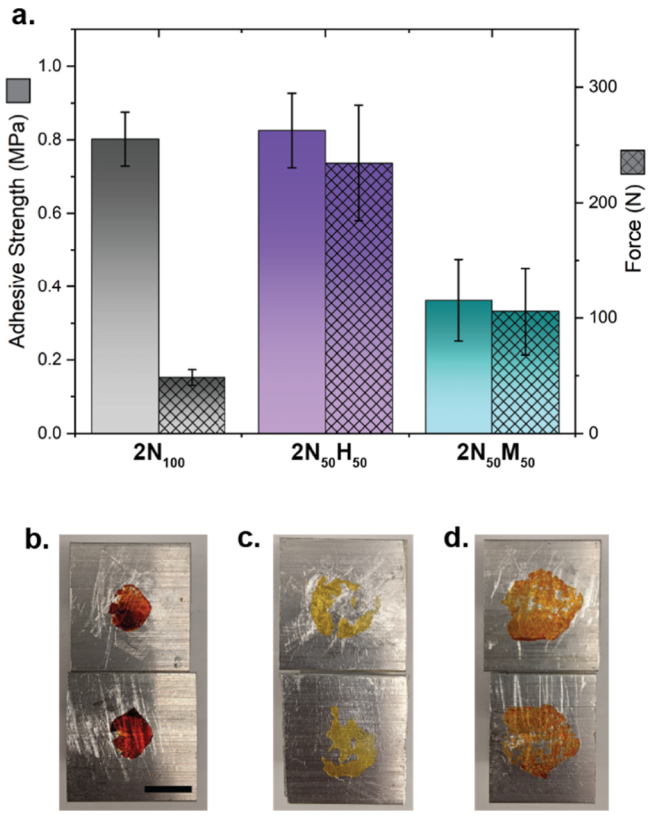

Figure 9. (a) Graphical comparison of adhesive strength of $\mathbf{2N_{100}}$ (gray), $\mathbf{2N_{50}H_{50}}$ (violet), and $\mathbf{2N_{50}M_{50}}$ (cyan) binding two aluminum substrates adhered at 180 °C (strain rate = 1 mm/min). Representative photographs of hot melt samples after failure, all demonstrating cohesive failure: (b) $\mathbf{2N_{100}}$, (c) $\mathbf{2N_{50}H_{50}}$, and (d) $\mathbf{2N_{50}M_{50}}$ (scale bar = 1 cm).

and peel tests verified that the dynamic networks were able to perform well as PSAs. In addition to their PSA properties, the phase-separated morphology of the adhesive networks made them candidates for HMAs. The different degrees of phase separation produced starkly different adhesive strengths in this context, with the highly phase-separated $\mathbf{2N_{50}H_{50}}$ material showing significantly enhanced HMA performance. Ongoing research seeks to better understand the DRIPS process as a function of thermal annealing conditions and polythiol architecture.

EXPERIMENTAL SECTION

Materials. **PMMS** homopolymer (4−7k Da) was purchased from Gelest and used without further purification. All other reagents were purchased from Sigma-Aldrich. Solvents for reactions and film casting were purchased from Fisher Scientific. Deuterated solvents were purchased from ACROS Organics. All chemicals were used as received without further purification unless otherwise noted.

Synthesis of Bisbenzalcyanoacrylate Compounds. The ditopic compounds were synthesized in two steps as previously described.[38,50] In the first step, the bis(cyanoacetate) core, triethylene glycol (TEG, 20.0 g, 0.13 mol, 0.78 M), and cyanoacetic acid (23.2 g, 0.27 mol) were combined in a 500 mL round-bottom flask with 0.12 M equivalents of catalytic *p*-toluenesulfonic acid monohydrate (3.0 g, 0.016 mol) in toluene (166.7 mL). The setup was equipped with a waterless condenser and a Dean−Stark trap, heated to 105 °C under a nitrogen atmosphere, and stirred using a magnetic stir bar for ca. 18 h (overnight). Once complete, the solvent was removed via rotary evaporation. The resulting yellow oil was diluted with ca. 300 mL of methylene chloride (DCM), and the remaining salts were filtered out. The filtrate was washed thoroughly (three or more times) with brine (sodium chloride-saturated water) and dried with magnesium sulfate. DCM was removed from the solution via rotary evaporation, and the resulting yellow oil was dried overnight under high vacuum (MW = 284.15 g/mol, yield = 70% by mass). ^{1}H NMR [500 MHz in $CDCl_3$; δ ppm: 3.54 (s, 2H), 3.68 (s, 2H), 3.76 (t, 2H), and 4.39 (t, 2H)]. ^{13}C NMR (101 MHz in $CDCl_3$; δ 163.11, 112.99, 70.68, 68.62, 65.77, 24.73).

*TEG Bis(4-nitrobenzalcyanoacrylate) (**1N**).* TEG bis(cyanoacetate) (1, 5 g, 0.018 mol, 0.14 M) and 4-nitrobenzaldehyde (5.74 g, 0.038 mol) were added a 250 mL round-bottom flask with DCM (130 mL) and 0.15 M equivalents of catalytic triethylamine (TEA, 0.3 mL, 0.003 mol). The flask was then placed under a nitrogen atmosphere and allowed to stir using a magnetic stir bar overnight. DCM was removed using rotary evaporation, and the resultant oil was triturated in MeOH for 2 h. The solution was filtered, and a solid powder was collected. This trituration process was repeated until the filtrate was clear and colorless, leaving behind a reddish, clumpy powder. ^{1}H NMR [500 MHz in $CDCl_3$; δ ppm: 3.77 (s, 2H), 3.89 (t, 2H), 4.54 (t, 2H), 8.16 (d, 2H), 8.34 (s, 1H), and 8.37 (d, 2H)]. ^{13}C NMR (126 MHz in $CDCl_3$; δ 161.95, 152.06, 149.78, 136.82, 131.59, 124.36, 114.36, 106.90, 53.90), and MALDI-MS (573.46, [M] + Na^+). Yield by mass = 45%.

*TEG Bis(benzalcyanoacrylate) (**1H**).* TEG bis(cyanoacetate) (1, 5.00 g, 0.018 mol, 0.14 M) and benzaldehyde (4.03 g, 0.038 mol) were added to a 250 mL round-bottom flask with DCM (130 mL) and 0.15 M equivalents of catalytic TEA (0.3 mL, 0.003 mol). The flask was then placed under a nitrogen atmosphere and allowed to stir using a magnetic stir bar overnight. DCM was removed using rotary evaporation, and the resultant oil was triturated in MeOH for 2 h. The solution was filtered, and a solid powder was collected. This trituration process was repeated until the filtrate was clear and colorless. ^{1}H NMR [500 MHz in $CDCl_3$; δ ppm: 3.77 (s, 2H), 3.88 (t, 2H), 4.51 (t, 2H), 7.53 (t, 2H), 7.58 (t, 1H), 8.01 (d, 2H) and 8.28 (s, 1H)]. ^{13}C NMR (101 MHz in $CDCl_3$; δ 162.51, 155.35, 133.40, 131.45, 131.15, 129.30, 115.36, 102.80, 70.91, 68.80, 65.81). Yield by mass = 51%.

*TEG Bis(4-methoxybenzalcyanoacrylate) (**1M**).* TEG bis(cyanoacetate) (**1**, 5.00 g, 0.018 mol, 0.14 M) and 4-methoxybenzaldehyde (5.17 g, 0.038 mol) were added to a 250 mL round-bottom flask with DCM (130 mL) and 0.15 M equivalents of catalytic TEA (0.3 mL, 0.003 mol). The flask was then placed under a nitrogen atmosphere and allowed to stir using a magnetic stir bar overnight. DCM was removed using rotary evaporation, and the resultant oil was triturated in MeOH for 2 h. The solution was filtered, and a solid powder was collected. This trituration process was repeated until the filtrate was clear and colorless. ^{1}H NMR [500 MHz in $CDCl_3$; δ ppm: 3.77 (s, 2H), 3.87 (t, 2H), 3.91 (s, 3H), 4.48 (t, 2H), 7.01 (d, 2H), 8.02 (d, 2H), and 8.20 (s, 1H)]. ^{13}C NMR (101 MHz in $CDCl_3$; δ 163.86, 163.14, 154.66, 133.74, 124.36, 116.08, 114.79, 99.14, 70.90, 68.87, 65.54, 55.64). Yield by mass = 51%.

*Synthesis of tM Networks (**2**).* tM networks were prepared following previously reported methods with minor modifications. Briefly, ditopic Michael acceptors (**1**, Figure 1c) and **PMMS** (Figure 1c) were dissolved in chloroform, stirred for 2 h at 50 °C, and cast onto Teflon drying dishes. The films were dried overnight at room temperature and then transferred to a vacuum oven at 60 °C and dried under reduced pressure for 24 h. The networks were then heated to 150 °C and held isothermally under a reduced pressure for 30 min to remove any trapped solvent before compression molding. The sample films were pressed at 70 °C for 10 min under 10 kpsi (films containing only **1N** were pressed at 90−120 °C). In total, three tM networks were prepared: $\mathbf{2N_{100}}$ as well as two hybrid materials composed of **1N** with **1H** ($\mathbf{2N_{50}H_{50}}$) and **1N** with **1M** ($\mathbf{2N_{50}M_{50}}$). The subscript denotes the mole percent (mol %) of each acceptor (x = 100 or 50) relative to the total amount of thiol.

Thermogravimetric Aanalysis. Thermogravimetric analysis was performed using a TA Instruments Discovery thermogravimetric analyzer in the Soft Matter Characterization Facility at the University of Chicago. Samples were tested under a nitrogen atmosphere using

https://doi.org/10.1021/acsami.1c05813
ACS Appl. Mater. Interfaces 2021, 13, 27471−27480

platinum pans. Tests were conducted using a ramp of 10 °C/min from the starting operating temperature (ca. 35 °C) to 600 °C.

Nuclear Magnetic Resonance. Nuclear magnetic resonance (NMR) was performed using a 500 MHz Bruker AVANCE II+ 500 11.7 T NMR or a Bruker AVANCE III HD 500 11.7 T NMR spectrometer at the NMR facilities at the University of Chicago. For experimental temperatures in the range of 25−45 °C, a standard plastic sample spinner was used; for equilibrium measurements at or above 55 °C, a ceramic spinner was used. Sample temperatures were measured through the use of an ethylene glycol standard;[51] see the Supporting Information for further information.

DSC. DSC was performed using a TA Instruments Discovery 2500 differential scanning calorimeter in the Soft Matter Characterization Facility at the University of Chicago. Samples were prepared in aluminum hermetic pans from TA Instruments and were hermetically sealed. Typical test conditions involved a cool−heat−cool−heat procedure from (−20 °C/200 °C/−80 °C/200 °C) with a rate of 10 °C/min.

Rheology. Rheology was performed using a TA Instruments RSA-G2 ARES rheometer with a forced convection oven (20−500 °C) attached to an air chiller system (−120−20 °C) and running TA Trios software in the Soft Matter Characterization Facility at the University of Chicago. An 8 mm stainless steel parallel plate was used for all tests. For frequency sweeps, the sample was equilibrated at the testing temperature for 5 min before the experiment was started. After equilibration, a frequency sweep from 0.01 to 100.0 rad/s was done at 1.0% strain. Subsequent sweeps were conducted by increasing the temperature by 5 °C and re-equilibrating for 5 min before beginning the frequency experiment.

Tensile Analysis. Tensile analysis was performed using a Zwick-Roell zwickiLine Z0.5 materials testing instrument with either a 100 N (peel tests) or 500 N (hot melt tests) load cell in the Soft Matter Characterization Facility at the University of Chicago.

AFM. AFM images were collected using an Asylum Research Cypher ES Environmental microscope. Tapping-mode imaging was performed using Asylum Research FS-1500-AuD cantilevers with resonant frequencies of 1.5 MHz. Images were collected at a scan rate of 2 Hz (for $\mathbf{2N_{100}}$) or 5 Hz (for $\mathbf{2N_{50}M_{50}}$ and $\mathbf{2N_{50}H_{50}}$) with a 500 mV set point in the repulsive mode (to prevent tip-induced damage of the sample surface). To achieve adequate phase contrast/image clarity, samples were imaged at 35 °C (for $\mathbf{2N_{100}}$) or 0 °C (for $\mathbf{2N_{50}M_{50}}$ and $\mathbf{2N_{50}H_{50}}$) in an argon atmosphere with cell gauge pressures of 30 mbarg. Samples were equilibrated for 5 min at the desired temperature prior to imaging. Images were processed with a first-order flatten.

Preparation of tM Adhesive Tapes. The film of interest was pressed between two Kapton sheets at 200 °C and 1 kpsi for 10 min, creating an adhesive layer that was approximately 100 μm thick. Tapes were cooled to room temperature on the benchtop and stored at −20 °C until needed.

Tack Tests. The tack of the TM tapes was evaluated using a TA Instruments ARES-G2 rheometer equipped with an 8 mm stainless steel parallel plate. Samples were cut in 8 mm × 8 mm squares and mounted onto the lower plate using double-sided tape. An axial force (0.1 N, 1.0 N, or 10 N) was applied to the sample for a predetermined period of time (20 s, 60 s, or 120 s) after which the upper plate was removed from the adhesive at a constant rate of 0.1 mm/s.

180° Peel Tests. The adhesive tape was cut into a strip ca. 5 mm wide and 70 mm long. The strip was adhered to a glass microscope slide using a strong cyanoacrylate-based adhesive. The free Kapton surface was removed immediately prior to testing, and a strip of aluminum foil (approximately 10 mm wide and 200 mm long) was adhered to the tM adhesive by rolling with a weighted 1 kg roller (taking care to not exert additional force onto the sample). The aluminum foil was folded in half, and the setup was mounted into the Zwick grips. Peel tests were run for a travel distance of 50 mm at a strain rate of 10 mm/min.

Hot Melt Adhesion Tests. A 5 mm × 5 mm square of the original pressed films (not tape) was situated between two aluminum I-bars which were then clamped together with clips. The entire setup was placed in an oven at 180 °C for 10 min after which it was removed and allowed to cool on the benchtop with the clips attached for another 10 min. Once cooled, the clips were removed, and the adhered I-bars were loaded onto the Zwick clamps. Adhesive strength of the hot melt bond was measured at 1 mm/min, and the area used for calculating the adhesive strength was estimated from the average area of the circular adhesive footprint left after the bond failed.

■ ASSOCIATED CONTENT

Supporting Information

The Supporting Information is available free of charge at https://pubs.acs.org/doi/10.1021/acsami.1c05813.

Additional characterization of adhesive networks including TGA, DSC, temperature-dependent NMR methods, and spectra, AFM height traces, SAOS frequency sweeps, and adhesive test results (PDF)

■ AUTHOR INFORMATION

Corresponding Author

Stuart J. Rowan − *Pritzker School of Molecular Engineering and Department of Chemistry, University of Chicago, Chicago, Illinois 60637, United States; Chemical Science and Engineering Division and Center for Molecular Engineering, Argonne National Laboratory, Lemont, Illinois 60434, United States;* orcid.org/0000-0001-8176-0594; Email: stuartrowan@uchicago.edu

Authors

Katie M. Herbert − *Pritzker School of Molecular Engineering, University of Chicago, Chicago, Illinois 60637, United States;* orcid.org/0000-0002-4640-4225

Neil D. Dolinski − *Pritzker School of Molecular Engineering, University of Chicago, Chicago, Illinois 60637, United States*

Nicholas R. Boynton − *Pritzker School of Molecular Engineering, University of Chicago, Chicago, Illinois 60637, United States*

Julia G. Murphy − *Department of Chemistry and James Franck Institute, University of Chicago, Chicago, Illinois 60637, United States*

Charlie A. Lindberg − *Pritzker School of Molecular Engineering, University of Chicago, Chicago, Illinois 60637, United States*

S. J. Sibener − *Department of Chemistry and James Franck Institute, University of Chicago, Chicago, Illinois 60637, United States*

Complete contact information is available at: https://pubs.acs.org/10.1021/acsami.1c05813

Notes

The authors declare no competing financial interest.

■ ACKNOWLEDGMENTS

This work was supported by the Division of Materials Research of the NSF (award #1609076) and in part by NIST contract 60NANB15D077, the Center for Hierarchical Materials Design (CHiMaD), and the University of Chicago Materials Research Science and Engineering Center (MRSEC) (award #DMR-2011854). N.D.D. thanks the Pritzker School of Molecular Engineering for support through a postdoctoral fellowship. Parts of this work were carried out at the Soft Matter Characterization Facility and at the MRSEC Characterization Facility at the University of Chicago (award number DMR-2011854).

REFERENCES

(1) Kato, R.; Mirmira, P.; Sookezian, A.; Grocke, G. L.; Patel, S. N.; Rowan, S. J. Ion-Conducting Dynamic Solid Polymer Electrolyte Adhesives. *ACS Macro Lett.* **2020**, *9*, 500−506.

(2) Wang, Y.; Gozen, A.; Chen, L.; Zhong, W. H. Gum-Like Nanocomposites as Conformable, Conductive, and Adhesive Electrode Matrix for Energy Storage Devices. *Adv. Energy Mater.* **2017**, 71601767, DOI: DOI: 10.1002/aenm.201601767.

(3) Li, Z.; Le, T.; Wu, Z.; Yao, Y.; Li, L.; Tentzeris, M.; Moon, K.-S.; Wong, C. P. Rational Design of a Printable, Highly Conductive Silicone-Based Electrically Conductive Adhesive for Stretchable Radio-Frequency Antennas. *Adv. Funct. Mater.* **2015**, *25*, 464−470.

(4) Kim, H. J.; Paquin, L.; Barney, C. W.; So, S.; Chen, B.; Suo, Z.; Crosby, A. J.; Hayward, R. C. Low-Voltage Reversible Electroadhesion of Ionoelastomer Junctions. *Adv. Mater.* **2020**, *32*, 2000600.

(5) Jing, X.; Mi, H.-Y.; Lin, Y.-J.; Enriquez, E.; Peng, X.-F.; Turng, L.-S. Highly Stretchable and Biocompatible Strain Sensors Based on Mussel-Inspired Super-Adhesive Self-Healing Hydrogels for Human Motion Monitoring. *ACS Appl. Mater. Interfaces* **2018**, *10*, 20897−20909.

(6) Yang, Y.; Qi, P.; Ding, Y.; Maitz, M. F.; Yang, Z.; Tu, Q.; Xiong, K.; Leng, Y.; Huang, N. A Biocompatible and Functional Adhesive Amine-Rich Coating Based on Dopamine Polymerization. *J. Mater. Chem. B* **2015**, *3*, 72−81.

(7) Assmann, A.; Vegh, A.; Ghasemi-Rad, M.; Bagherifard, S.; Cheng, G.; Sani, E. S.; Ruiz-Esparza, G. U.; Noshadi, I.; Lassaletta, A. D.; Gangadharan, S.; Tamayol, A.; Khademhosseini, A.; Annabi, N. A Highly Adhesive and Naturally Derived Sealant. *Biomaterials* **2017**, *140*, 115−127.

(8) Kang, J.-S.; Myles, A. J.; Harris, K. D. Thermally-Degradable Thermoset Adhesive Based on a Cellulose Nanocrystals/Epoxy Nanocomposite. *ACS Appl. Polym. Mater.* **2020**, *2*, 4626−4631.

(9) Kaminker, R.; Callaway, E. B.; Dolinski, N. D.; Barbon, S. M.; Shibata, M.; Wang, H.; Hu, J.; Hawker, C. J. Solvent-Free Synthesis of High-Performance Polyhexahydrotriazine (PHT) Thermosets. *Chem. Mater.* **2018**, *30*, 8352−8358.

(10) Bhagat, V.; Becker, M. L. Degradable Adhesives for Surgery and Tissue Engineering. *Biomacromolecules* **2017**, *18*, 3009−3039.

(11) Zhang, H.; Zhao, T.; Duffy, P.; Dong, Y.; Annaidh, A. N.; O'Cearbhaill, E.; Wang, W. Hydrolytically Degradable Hyperbranched PEG-Polyester Adhesive with Low Swelling and Robust Mechanical Properties. *Adv. Healthcare Mater.* **2015**, *4*, 2260−2268.

(12) Kim, H.; Mohapatra, H.; Phillips, S. T. Rapid, On-Command Debonding of Stimuli-Responsive Cross-Linked Adhesives by Continuous, Sequential Quinone Methide Elimination Reactions. *Angew. Chem., Int. Ed.* **2015**, *54*, 13063−13067.

(13) Chan, E. P.; Smith, E. J.; Hayward, R. C.; Crosby, A. J. Surface Wrinkles for Smart Adhesion. *Adv. Mater.* **2008**, *20*, 711−716.

(14) Hwang, D.-G.; Trent, K.; Bartlett, M. D. Kirigami-Inspired Structures for Smart Adhesion. *ACS Appl. Mater. Interfaces* **2018**, *10*, 6747−6754.

(15) Benedek, I. *Pressure-Sensitive Adhesives and Applications*, 2nd ed.; CRC Press: New York, NY, 2004.

(16) Creton, C. Pressure-Sensitive Adhesives: An Introductory Course. *MRS Bull.* **2003**, *28*, 434−439.

(17) Skeist, I. *Handbook of Adhesives*, 3rd ed.; Chapman & Hall: New York, 1989.

(18) Lafont, U.; van Zeijl, H.; van der Zwaag, S. Influence of Cross-Linkers on the Cohesive and Adhesive Self-Healing Ability of Polysulfide-Based Thermosets. *ACS Appl. Mater. Interfaces* **2012**, *4*, 6280−6288.

(19) Meng, Y. Z.; Tjong, S. C.; Hay, A. S. Synthesis of Cocyclic(Arylene Disulfide) Oligomers and Their Adhesion Properties as Heating-Melt Adhesive. *Polymer* **2001**, *42*, 5215−5224.

(20) Abdolah Zadeh, M.; van der Zwaag, S.; Garcia, S. J. Adhesion and Long-Term Barrier Restoration of Intrinsic Self-Healing Hybrid Sol−Gel Coatings. *ACS Appl. Mater. Interfaces* **2016**, *8*, 4126−4136.

(21) Aubert, J. H. Note: Thermally Removable Epoxy Adhesives Incorporating Thermally Reversible Diels-Alder Adducts. *J. Adhes.* **2003**, *79*, 609−616.

(22) Heinzmann, C.; Weder, C.; De Espinosa, L. M. Supramolecular Polymer Adhesives: Advanced Materials Inspired by Nature. *Chem. Soc. Rev.* **2016**, *45*, 342−358.

(23) Michal, B. T.; Spencer, E. J.; Rowan, S. J. Stimuli-Responsive Reversible Two-Level Adhesion from a Structurally Dynamic Shape-Memory Polymer. *ACS Appl. Mater. Interfaces* **2016**, *8*, 11041−11049.

(24) Cudjoe, E.; Herbert, K. M.; Rowan, S. J. Strong, Rebondable, Dynamic Cross-Linked Cellulose Nanocrystal Polymer Nanocomposite Adhesives. *ACS Appl. Mater. Interfaces* **2018**, *10*, 30723−30731.

(25) Courtois, J.; Baroudi, I.; Nouvel, N.; Degrandi, E.; Pensec, S.; Ducouret, G.; Chanéac, C.; Bouteiller, L.; Creton, C. Supramolecular Soft Adhesive Materials. *Adv. Funct. Mater.* **2010**, *20*, 1803−1811.

(26) Arrington, K. J.; Radzinski, S. C.; Drummey, K. J.; Long, T. E.; Matson, J. B. Reversibly Cross-Linkable Bottlebrush Polymers as Pressure-Sensitive Adhesives. *ACS Appl. Mater. Interfaces* **2018**, *10*, 26662−26668.

(27) Zhang, K.; Fahs, G. B.; Margaretta, E.; Hudson, A. G.; Moore, R. B.; Long, T. E. Acetyl-Protected Cytosine and Guanine Containing Acrylics as Supramolecular Adhesives. *J. Adhes.* **2019**, *95*, 146−167.

(28) Chakma, P.; Konkolewicz, D. Dynamic Covalent Bonds in Polymeric Materials. *Angew. Chem., Int. Ed.* **2019**, *58*, 9682−9695.

(29) Jin, Y.; Yu, C.; Denman, R. J.; Zhang, W. Recent Advances in Dynamic Covalent Chemistry. *Chem. Soc. Rev.* **2013**, *42*, 6634−6654.

(30) Rowan, S. J.; Cantrill, S. J.; Cousins, G. R. L.; Sanders, J. K. M.; Stoddart, J. F. Dynamic Covalent Chemistry. *Angew. Chem., Int. Ed.* **2002**, *41*, 898−952.

(31) Kloxin, C. J.; Scott, T. F.; Adzima, B. J.; Bowman, C. N. Covalent Adaptable Networks (CANs): A Unique Paradigm in Cross-Linked Polymers. *Macromolecules* **2010**, *43*, 2643−2653.

(32) Li, L.; Chen, X.; Torkelson, J. M. Covalent Adaptive Networks for Enhanced Adhesion: Exploiting Disulfide Dynamic Chemistry and Annealing during Application. *ACS Appl. Polym. Mater.* **2020**, *2*, 4658−4665.

(33) Tsai, H.-Y.; Nakamura, Y.; Fujita, T.; Naito, M. Strengthening Epoxy Adhesives at Elevated Temperatures Based on Dynamic Disulfide Bonds. *Mater. Adv.* **2020**, *1*, 3182−3188.

(34) Ji, F.; Liu, X.; Sheng, D.; Yang, Y. Epoxy-Vitrimer Composites Based on Exchangeable Aromatic Disulfide Bonds: Reprocessibility, Adhesive, Multi-Shape Memory Effect. *Polymer* **2020**, *197*, 122514.

(35) Dobson, A. L.; Bongiardina, N. J.; Bowman, C. N. Combined Dynamic Network and Filler Interface Approach for Improved Adhesion and Toughness in Pressure-Sensitive Adhesives. *ACS Appl. Polym. Mater.* **2020**, *2*, 1053−1060.

(36) Zhong, Y.; Xu, Y.; Anslyn, E. V. Studies of Reversible Conjugate Additions. *Eur. J. Org. Chem.* **2013**, *2013*, 5017−5021.

(37) Serafimova, I. M.; Pufall, M. A.; Krishnan, S.; Duda, K.; Cohen, M. S.; Maglathlin, R. L.; McFarland, J. M.; Miller, R. M.; Frödin, M.; Taunton, J. Reversible Targeting of Noncatalytic Cysteines with Chemically Tuned Electrophiles. *Nat. Chem. Biol.* **2012**, *8*, 471.

(38) Herbert, K. M.; Getty, P. T.; Dolinski, N. D.; Hertzog, J. E.; de Jong, D.; Lettow, J. H.; Romulus, J.; Onorato, J. W.; Foster, E. M.; Rowan, S. J. Dynamic Reaction-Induced Phase Separation in Tunable, Adaptive Covalent Networks. *Chem. Sci.* **2020**, *11*, 5028−5036.

(39) Fitzsimons, T. M.; Oentoro, F.; Shanbhag, T. V.; Anslyn, E. V.; Rosales, A. M. Preferential Control of Forward Reaction Kinetics in Hydrogels Crosslinked with Reversible Conjugate Additions. *Macromolecules* **2020**, *53*, 3738−3746.

(40) Zhang, B.; Digby, Z. A.; Chakma, P.; Sparks, J. L.; Konkolewicz, D.; Sparks, L.; Konkolewicz, D. Dynamic Thiol−Michael Chemistry for Thermoresponsive Rehealable and Malleable Networks. *Macromolecules* **2016**, *49*, 6871−6878.

(41) Chakma, P.; Rodrigues Possarle, L. H.; Digby, Z. A.; Zhang, B.; Sparks, J. L.; Konkolewicz, D. Dual Stimuli Responsive Self-Healing and Malleable Materials Based on Dynamic Thiol-Michael Chemistry. *Polym. Chem.* **2017**, *8*, 6534−6543.

https://doi.org/10.1021/acsami.1c05813
ACS Appl. Mater. Interfaces 2021, 13, 27471−27480

(42) Van Herck, N.; Maes, D.; Unal, K.; Guerre, M.; Winne, J. M.; Du Prez, F. E. Covalent Adaptable Networks with Tunable Exchange Rates Based on Reversible Thiol-yne Cross-Linking. *Angew. Chem., Int. Ed.* **2020**, *59*, 3609−3617.
(43) Kuhl, N.; Geitner, R.; Bose, R. K.; Bode, S.; Dietzek, B.; Schmitt, M.; Popp, J.; Garcia, S. J.; van der Zwaag, S.; Schubert, U. S.; Hager, M. D. Self-Healing Polymer Networks Based on Reversible Michael Addition Reactions. *Macromol. Chem. Phys.* **2016**, *217*, 2541−2550.
(44) Kuhl, N.; Geitner, R.; Vitz, J.; Bode, S.; Schmitt, M.; Popp, J.; Schubert, U. S.; Hager, M. D. Increased Stability in Self-Healing Polymer Networks Based on Reversible Michael Addition Reactions. *J. Appl. Polym. Sci.* **2017**, *134*, 44805.
(45) Baldwin, A. D.; Kiick, K. L. Reversible Maleimide-Thiol Adducts Yield Glutathione-Sensitive Poly(Ethylene Glycol)-Heparin Hydrogels. *Polym. Chem.* **2013**, *4*, 133−143.
(46) Kharkar, P. M.; Kiick, K. L.; Kloxin, A. M. Design of Thiol- and Light-Sensitive Degradable Hydrogels Using Michael-Type Addition Reactions. *Polym. Chem.* **2015**, *6*, 5565−5574.
(47) Lin, S. B.; Durfee, L. D.; Ekeland, R. A.; McVie, J.; Schalau, G. K. Recent Advances in Silicone Pressure-Sensitive Adhesives. *J. Adhes. Sci. Technol.* **2007**, *21*, 605−623.
(48) Dahlquist, C. A. Pressure-Sensitive Adhesives. *Treatise on Adhesion Adhesives*; Marcel Dekker, Inc., 1969; Vol. 2, pp 219−260.
(49) Chang, E. P. Viscoelastic Windows of Pressure-Sensitive Adhesives. *J. Adhes.* **1991**, *34*, 189−200.
(50) Sassi, T. P.; Gupta, R. B. Dimeric Cyanoacrylate Compounds as Red-Shifted UV Absorbers. WO 2010056452 A2, 2009.
(51) Ammann, C.; Meier, P.; Merbach, A. A Simple Multinuclear NMR Thermometer. *J. Magn. Reson.* **1982**, *46*, 319−321.

https://doi.org/10.1021/acsami.1c05813
ACS Appl. Mater. Interfaces 2021, 13, 27471−27480